*Bull Mater Sci* (2021)44:11
https://doi.org/10.1007/s12034-020-02313-1



# Study of optical properties of $TiO_2$ nanoparticles and CdS@$TiO_2$ nanocomposites and their use for photocatalytic degradation of rhodamine B under natural light irradiation

**RASHMI A BADHE, ALEEM ANSARI and SHIVRAM S GARJE***
Department of Chemistry, University of Mumbai, Vidyanagari, Santacruz (East), Mumbai 400098, India
*Author for correspondence (ssgarje@chem.mu.ac.in; ssgarje@yahoo.com)

MS received 10 June 2020; accepted 14 August 2020

**Abstract.** In this study, we report the synthesis of two CdS@$TiO_2$ nanocomposites (CT1 and CT2) by two-step low temperature solvothermal decomposition method using two different stoichiometric combinations between CdS and $TiO_2$ nanoparticles (NPs). $CdCl_2$(3-chlorobenzaldehyde thiosemicarbazone)$_2$ was used as a molecular precursor to obtain CdS NPs, whereas titanium isopropoxide was used to obtain $TiO_2$ NPs. The as-prepared CT nanocomposites were characterized by powder X-ray diffraction, field emission scanning electron microscopy, Raman spectroscopy, transmission electron microscopy and X-ray photoelectron spectroscopy to evaluate their structures and properties. Further, these nanocomposites were used for the photocatalytic degradation of rhodamine B under solar light irradiation. It is found that CdS@$TiO_2$ (CT1) nanocomposite shows highest degradation efficiency of 98.74% within 60 min as compared to bare $TiO_2$ NPs which shows only 66.40% degradation efficiency. The enhanced photocatalytic efficiency due to charge transfer properties of bare NPs and CT nanocomposites was further investigated by electrochemical analysis and photoluminescence studies.

**Keywords.** Molecular precursor; solvothermal method; composite materials; optical properties; photocatalytic activity.

## 1. Introduction

The organic pollutants, hazardous materials and industrial toxic effluents in waste water have major environmental issues. To overcome these problems, development of most promising materials for water purification has great significance [1]. For the removal of organic dyes, a major pollutant, various metal oxide semiconductor nanoparticles (NPs), such as $TiO_2$, ZnS, CdS, $Fe_2O_3$ and ZnO have been used. Among these, $TiO_2$ NPs have excellent properties for the photodegradation of organic pollutants and toxic dyes [2]. It has been mostly recognized semiconductor material for the industrial application, because of its high photocatalytic activity, chemical inertness, high stability, low cost and non-toxicity [3–6]. However, due to its wide band gap (anatase $E_g$ = 3.2 eV; rutile $E_g$ = 3.0 eV), it has some limitations as a photocatalyst. This is because only 3–5% of the solar light spectrum falls in the UV region, which restricts the photocatalytic activity of $TiO_2$ in the solar region [7–9]. To enhance the use of solar energy spectrum in photocatalysis by semiconductor materials, several methods have been reported, such as doping of semiconductors with nitrogen, tin [10], transition metals [11–13] or combining them with another narrow band-gap semiconductors [14,15], etc. Among various narrow band-gap semiconductor materials, CdS is the most promising candidate due to its unique optical properties, which falls under visible region at wavelength of ~510 nm ($E_g$ = 2.42 eV) [16]. When CdS is coupled with $TiO_2$, resulting material shows excellent photocatalytic activity towards visible region due to generation of electrons and holes [17–20]. CdS@$TiO_2$ heterojunction nanocomposites (NCs), reduce the recombination rate of electron–hole pair, which is responsible for enhancing the light harvesting efficiency of photocatalysts. The improvement in photocatalytic activity of catalyst has been observed due to the synergetic effect between $TiO_2$ and CdS NPs [21].

Several researchers have reported the synthesis of CdS@$TiO_2$ nanocomposites using various methods, such as sol–gel [22], hydrothermal [9], silar method [23], chemical bath deposition [24], electrospining [7] and solvothermal method [1]. Very few reports are available on the synthesis of metal chalcogenide nanocomposites using molecular precursors. For example, Pawar *et al* [25] have reported the

*Electronic supplementary material: The online version of this article (https://doi.org/10.1007/s12034-020-02313-1) contains supplementary material, which is available to authorized users.*

Published online: 03 February 2021

synthesis of CdS–oxidized multiwalled carbon nanotube (OMWCNT) through a solvothermal route for the photodegradation of methylene blue dye, Samant *et al* [26] have prepared CSs–ZnS composite by solvothermal method, showing good photocatalytic activity for the photodegradation of eriochrome black-T and methylene blue. Earlier, we have reported synthesis of CdS@$TiO_2$ using solvothermal route and used it as a catalyst for the reduction of nitroaromatic compounds [27]. As the molecular precursors contain the desired elements in a single molecule, they have inherent advantages over other multiple source precursors, such as low toxicity, no or limited pre-reactions, control over stoichiometry, low volatility [28,29], etc.

In this study, CdS@$TiO_2$ (CT) nanocomposites were prepared via two-step low temperature solvothermal method. $TiO_2$ NPs were prepared using titanium isopropoxide precursor (first step). These $TiO_2$ NPs were further used for the synthesis of CdS@$TiO_2$ nanocomposites using $CdCl_2$(3-chlorobenzaldehyde thiosemicarbazone)$_2$ as a molecular precursor for CdS (second step). Further, the resulting materials have been used as photocatalysts for the degradation of rhodamine B (RhB) under solar light. Their charge transfer behaviour was studied by photoluminescence (PL), cyclic voltammetry (CV) and electrochemical impedance spectroscopy (EIS) studies.

## 2. Experimental

### 2.1 *Materials*

Titanium (IV) isopropoxide ≥97% and nafion were purchased from Sigma-Aldrich. Ethylene glycol, thiosemicarbazide, cadmium chloride ($CdCl_2$), potassium chloride (KCl) and 3-chlorobenzaldehyde were purchased from S.D. Fine Chemicals Limited. All chemicals purchased were of analytical grade and used without further purification. Double distilled water was used throughout the experiment.

### 2.2 *Synthesis of molecular precursor*

The molecular precursor was prepared according to the reported method [30]. 1.795 g (4.199 mmol) of 3-chlorobenzaldehyde thiosemicarbazone was dissolved in a mixture of anhydrous methanol and anhydrous THF (20 ml). Then this solution was added to the round bottom flask kept under nitrogen atmosphere containing solution of 0.770 g (4.200 mmol) cadmium chloride dissolved in anhydrous methanol (20 ml) kept under nitrogen atmosphere. To complete the reaction, the reaction mixture was allowed to stir for 48 h at room temperature. Then, the solvent was evaporated under vacuum to get a white product. Further, it was repeatedly washed with cyclohexane (3 × 10 ml) and n-hexane (3 × 10 ml) to remove any impurities if present. The resulting white product was dried under vacuum (MP: 227°C, yield: 2.348 g, 93.92%).

FTIR: 3434.03 $cm^{-1}$, 3262.99 $cm^{-1}$ ($\upsilon_{NH2}$ assym. and symm.); 3172.81 $cm^{-1}$ ($\upsilon_{NH}$); 1596.18 $cm^{-1}$ ($\upsilon_{C=N}$); 941.58 $cm^{-1}$ ($\upsilon_{C=S}$) (supplementary figure S1). $^1$H NMR: (300 MHz, [$D_6$] DMSO, 25°C, TMS): 7.4–8.2 (m, 7H, $-C_6H_5$ + $NH_2$); 11.5 (s, 1H, –NH) (supplementary figure S2a). $^{13}C\{^1H\}$ NMR (300 MHz, [$D_6$] DMSO, 25°C, TMS): 177.9 (>C=S); 140.7 (>C=N); 136.4–125.9 (aromatic carbons) (supplementary figure S2b).

### 2.3 *Synthesis of nanoparticles and nanocomposites*

2.3a *Synthesis of $TiO_2$ nanoparticles by solvothermal method* [31]*:* In a typical synthesis, 50 $cm^3$ of double distilled water was taken in a round bottom flask kept under nitrogen atmosphere and allowed to stir and refluxed. Then, 3 $cm^3$ of titanium isopropoxide precursor was injected with the help of syringe into the above refluxing solution. The reaction mixture was then refluxed for 2 h under nitrogen atmosphere. The reaction mixture was then allowed to cool to room temperature. The white product, i.e., obtained $TiO_2$ nanoparticles was separated by centrifugation. It was repeatedly washed 4–5 times with double distilled water and centrifuged to get the final material. The product was dried in oven at 70°C for 5 h. The obtained product was further characterized by various techniques.

2.3b *Synthesis of CdS@$TiO_2$ nanocomposites by solvothermal method:* In a typical synthesis, 350 mg $CdCl_2$(3-Cl-benztsczH)$_2$, (3-Cl-benztsczH = 3-chlorobenzaldehyde thiosemicarbazone) was taken in 50 ml ethylene glycol (EG) and sonicated for 30 min. After sonication, 50 mg (CT1) or 100 mg (CT2) of as pre-synthesized $TiO_2$ NPs were added. The solution was allowed to stir and reflux under nitrogen atmosphere for 2 h at 200°C. Then the reaction mixture was allowed to cool at room temperature under nitrogen atmosphere. The yellowish product, CdS@$TiO_2$ nanocomposites obtained was washed 4–5 times with methanol followed by centrifugation to remove excess of EG or any other impurities. The product was then dried under vacuum and further characterized.

### 2.4 *Characterization of $TiO_2$ NPs and CdS@$TiO_2$ nanocomposites*

The X-ray diffraction (XRD) studies were carried out on XRD-7000 Shimadzu X-ray diffractometer, using CuKα radiation with $\lambda$ = 0.15406 nm at a scan rate of 2° $min^{-1}$. The accelerating voltage and applied current were 20 kV and 20 mA, respectively. Fourier transform infrared (FTIR) spectra were recorded in the range of 400–4000 $cm^{-1}$ with Perkin Elmer FTIR spectrophotometer as KBr pellets using KBr press. The $^1$H and $^{13}C\{^1H\}$ nuclear magnetic resonance

(NMR) spectra were recorded in dimethyl sulphoxide-$d_6$ (DMSO-$d_6$) on Bruker Avance 300 spectrophotometer. The chemical shifts were referred to the internal standard tetramethyl silane (TMS) for both $^1$H and $^{13}$C{$^1$H} NMR spectra. The morphologies and elemental analysis of composites were performed using FEI make Nova NanoSEM 450 field emission scanning microscope (FESEM) with energy dispersive X-ray analysis (EDAX) using Bruker XFlash 6130 with operating voltage of 20 kV and EDAX, respectively. Transmission electron microscopy (TEM) and selected area electron diffraction (SAED) were recorded on PHILIPS, CM 200 microscope with operating voltage between 20 and 200 kV. The diffused reflectance spectra (DRS) were recorded using UV-2450 PC Shimadzu UV–Vis spectrophotometer at room temperature using $BaSO_4$ as reflectance standard. Raman spectra were recorded using Kaiser Optical systems Inc. (KOSI) laser Raman spectrometer. The X-ray photoelectron spectroscopy (XPS) measurements were performed on ESCA$^+$ omicron nanotechnology oxford instrument. C 1s peak with binding energy of 284.6 eV is used as an internal standard for the calibration of the binding energy scales. The fluorescence spectra were recorded on a Perkin Elmer LS 55 fluorescence spectrometer. The specific surface area was determined using nitrogen adsorption–desorption instrument (SMART SORB 92/93 BET). Brunauer–Emmet–Teller (BET) analysis is based on the single layer adsorption of $N_2$ gas at partial pressure ($p/p_0$ = 0.025–0.999). Before $N_2$ adsorption, all samples were degassed at 100°C. The electrochemical measurements, i.e., CV and EIS were carried out using AUT87573 equipped with USB electrochemical interface using Nova 2.1.3. The CV measurements were carried out using 1 M KCl aqueous electrolyte solution at a scan rate of 20 mV s$^{-1}$ in the potential range of 0.0–0.6 V. The EIS measurements were performed in the frequency range of 0.01 Hz–100 kHz with amplitude of 10 mV.

### 2.5 *Photocatalytic activity*

Photocatalytic performances of as-prepared NPs and NCs were evaluated through the degradation of RhB in an aqueous solution under solar light. Direct sunlight was used in this study and the experiment was carried out between 11.00 am and 2.00 pm, when solar intensity fluctuations were minimal. In a typical experiment, 10 mg l$^{-1}$ aqueous solution of RhB was prepared. Fifty milligrams of the sample as a catalyst was dispersed in 50 ml of aqueous solution containing RhB ($C_0$ = 10 mg l$^{-1}$). The mixture was sonicated for 10 min. The suspensions were magnetically stirred for 30 min in the dark to achieve adsorption–desorption equilibrium between dye and catalyst at room temperature. The dye and catalyst suspensions were magnetically stirred before and during the irradiation. During irradiation of aqueous dye solution, 3 ml of samples were extracted for analysis at every 15 min intervals. The photocatalysts were removed from solution by centrifugation and the supernatant was filtered through Whatman filter paper 41. The degradation of RhB was observed by measuring intensity of its absorption peak at 553 nm using a UV-2450 PC Shimadzu UV–Vis spectrophotometer. The recyclability of as-synthesized catalyst was studied up to 5 cycles under similar conditions. In this, the catalyst used in the previous cycle was separated by centrifugation, dried in oven and reused for the next cycle with fresh solution of RhB dye for the degradation studies. The photodegradation efficiency of RhB dye was calculated using formula $C/C_0$, where $C$ is the concentration of RhB solution at each irradiation time interval, and $C_0$ is the initial concentration when the adsorption–desorption equilibrium was achieved.

## 3. Results and discussion

Figure 1 shows XRD patterns of $TiO_2$ NPs and CdS@$TiO_2$ nanocomposites (CT1 and CT2). The appearance of sharp and intense peaks implies the crystallinity of NPs and NCs. The crystallinity is retained even after the formation of CT1 and CT2 nanocomposites. The diffraction peaks of bare $TiO_2$ at $2\theta$ = 25.2, 37.8, 48.0 and 62.2° were attributed to tetragonal phase of $TiO_2$ (JCPDS no. 021-1272) [32]. The existence of hexagonal CdS phase (JCPDS no. 041-1049) with diffraction peaks at $2\theta$ = 26.5, 28.2, 37.1, 44.0, 48.1, 52.0 and 66.8° have been reported in the literature [33]. Along with peaks due to $TiO_2$, peaks corresponding to CdS have also been observed in the XRD patterns of CT1 and CT2 nanocomposites. This confirms the successful formation of CdS@$TiO_2$ nanocomposites. The average crystallite size of $TiO_2$ NPs and CT nanocomposites were calculated using Scherrer's formula, $D = k\lambda/\beta \cos\theta$, where $k$ is the shape factor and has a typical value of 0.9, $\lambda$ is the wavelength of the X-rays (0.15406 nm), $\beta$ is the full width half

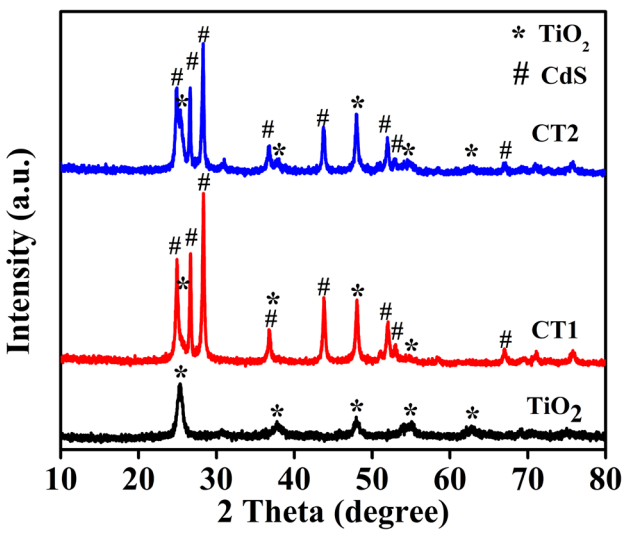


**Figure 1.** XRD patterns of as-synthesized bare $TiO_2$ NPs, CT1 and CT2 nanocomposites.

maximum (FWHM) of the most intense peaks and $\theta$ is the peak position [34]. For $TiO_2$ NPs, the crystallite size was calculated using peaks at $2\theta$ = 25.2, 37.8 and 48.0°, and it is found to be 8.95 nm. For CT1 peaks at $2\theta$ = 24.9, 26.6 and 28.2° were considered and the crystallite size was found to be 30.19 nm, whereas for CT2 peaks at $2\theta$ = 25.1, 26.6 and 28.2° were considered and the average crystallite size was found to be 26.21 nm.

The surface morphology of bare $TiO_2$ NPs, CT1 (figure 2a and b) and CT2 (supplementary figure S3) nanocomposites obtained from solvothermal method was analysed by FESEM. Almost spherical morphology was observed for as-prepared NPs and NCs. The rough surface of the CT nanocomposites indicates that $TiO_2$ NPs have been successfully deposited on the surface of CdS nanocrystallites. The elemental composition of nanocomposites is determined by EDAX analysis. Supplementary figure S4a and b shows EDAX spectra of CT1 and CT2 nanocomposites, respectively. The prominent peaks due to cadmium (Cd), sulphur (S), titanium (Ti) and oxygen (O) are observed due to the presence of CdS and $TiO_2$ in the CT nanocomposites.

The as-synthesized $TiO_2$ NPs and CT nanocomposites were further characterized by TEM analysis (figure 3). TEM image of bare $TiO_2$ NPs shows their spherical morphology (figure 3a). Figure 3c and e shows TEM images of CT nanocomposites. The formation of agglomerated spherical nanoclusters of CdS coated with nearly spherical $TiO_2$ NPs can be seen. Figure 3b, d and f represents the SAED patterns of as-synthesized bare $TiO_2$ NPs and CT nanocomposites. Presence of ring patterns in these images indicated the polycrystallinity of the materials. Their corresponding diffraction planes were calculated and they were found to match with planes present in XRD patterns.

Figure 4 shows Raman spectra of bare $TiO_2$ NPs and nanocomposites (CT1 and CT2). In case of $TiO_2$, the phononic lines are observed at 141.90, 398.11, 513.96 and 636.76 $cm^{-1}$. These peaks can be assigned to the $E1_g$, $B1_g$, $A1_g$+$B1_g$ and $E_g$, respectively, for anatase phase of $TiO_2$ NPs [35–37]. In case of nanocomposites, two additional Raman peaks are observed at 286.78, 594.37 (CT1) and 286.61, 577.21 $cm^{-1}$ (CT2) as shown in figure 4. The peaks observed at 286.78 and 286.61 $cm^{-1}$ in CT1 and CT2, respectively, can be ascribed to the longitudinal optical (1LO) modes of CdS, whereas peaks at higher values, i.e., 594.37 $cm^{-1}$ (for CT1) and 577.21 $cm^{-1}$ (for CT2) can be assigned to their overtones (2LO) [38]. The corresponding peaks match well with the bulk CdS Raman peaks [37,38] which confirm that the CdS@$TiO_2$ nanocomposites have been successfully formed.

The surface composition of bare $TiO_2$ NPs and CT nanocomposite was further studied by XPS technique. Figure 5 shows XPS survey scans of $TiO_2$ NPs and CT1 nanocomposite. XPS spectrum of CT2 nanocomposite is shown in supplementary figure S5. The presence of peaks due to Ti and O (in $TiO_2$ NPs), Ti, O, Cd and S in CT1 and CT2 nanocomposites can be clearly seen in their corresponding XPS spectra. Figure 5i(a) shows the XPS spectrum of bare $TiO_2$ NPs. The peaks at 459.1 and 464.9 eV corresponds to the Ti $2p_{3/2}$ and Ti $2p_{1/2}$ binding energies [37,39]. Figure 5i(b) shows the presence of O 1s peak at 529.7 eV, which is due to presence of lattice oxygen in $TiO_2$ [22,30,40,41]. The XPS spectrum of CT1 nanocomposite is shown in figure 5ii. Peaks due to Ti 2p, O 1s, Cd 3d and S 2p can be seen. Figure 5ii(a) represents XPS spectrum of Ti 2p peaks located at 458.5 and 464.2 eV binding energies corresponding to Ti $2p_{3/2}$ and Ti $2p_{1/2}$, respectively [37,39]. The peak located at 529.8 eV binding energy corresponds to O 1s (figure 5ii(b)). This confirms the existence of lattice oxygen of $TiO_2$ NPs [22,40,41]. Figure 5ii(c) shows Cd 3d peaks located at 405.74 and 412.31 eV binding energies corresponding to Cd $3d_{5/2}$ and Cd $3d_{3/2}$, respectively [42–44]. This reveals the presence of $Cd^{2+}$ ion. Figure 5ii(d) shows two peaks of S 2p which are located at

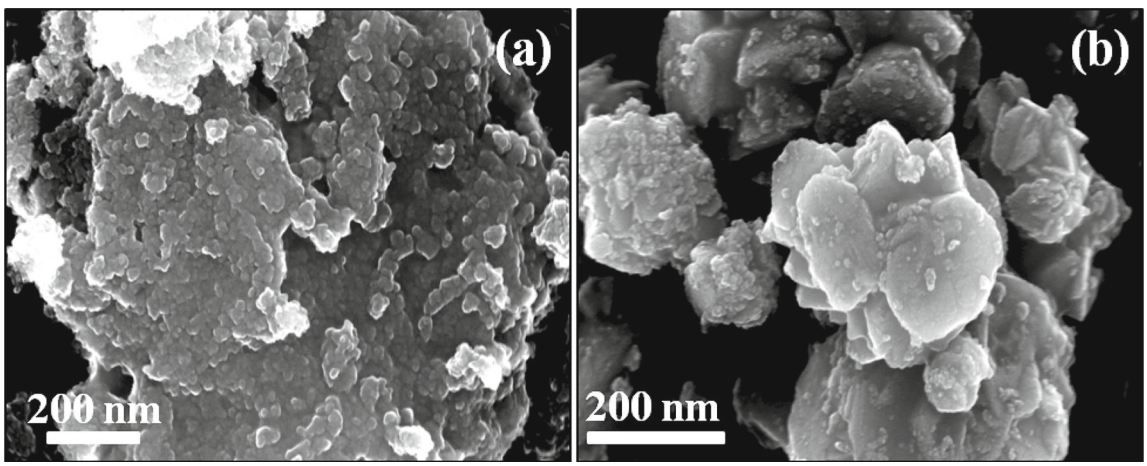


**Figure 2.** FESEM images of (**a**) as-synthesized bare $TiO_2$ NPs and (**b**) CT1 nanocomposite.

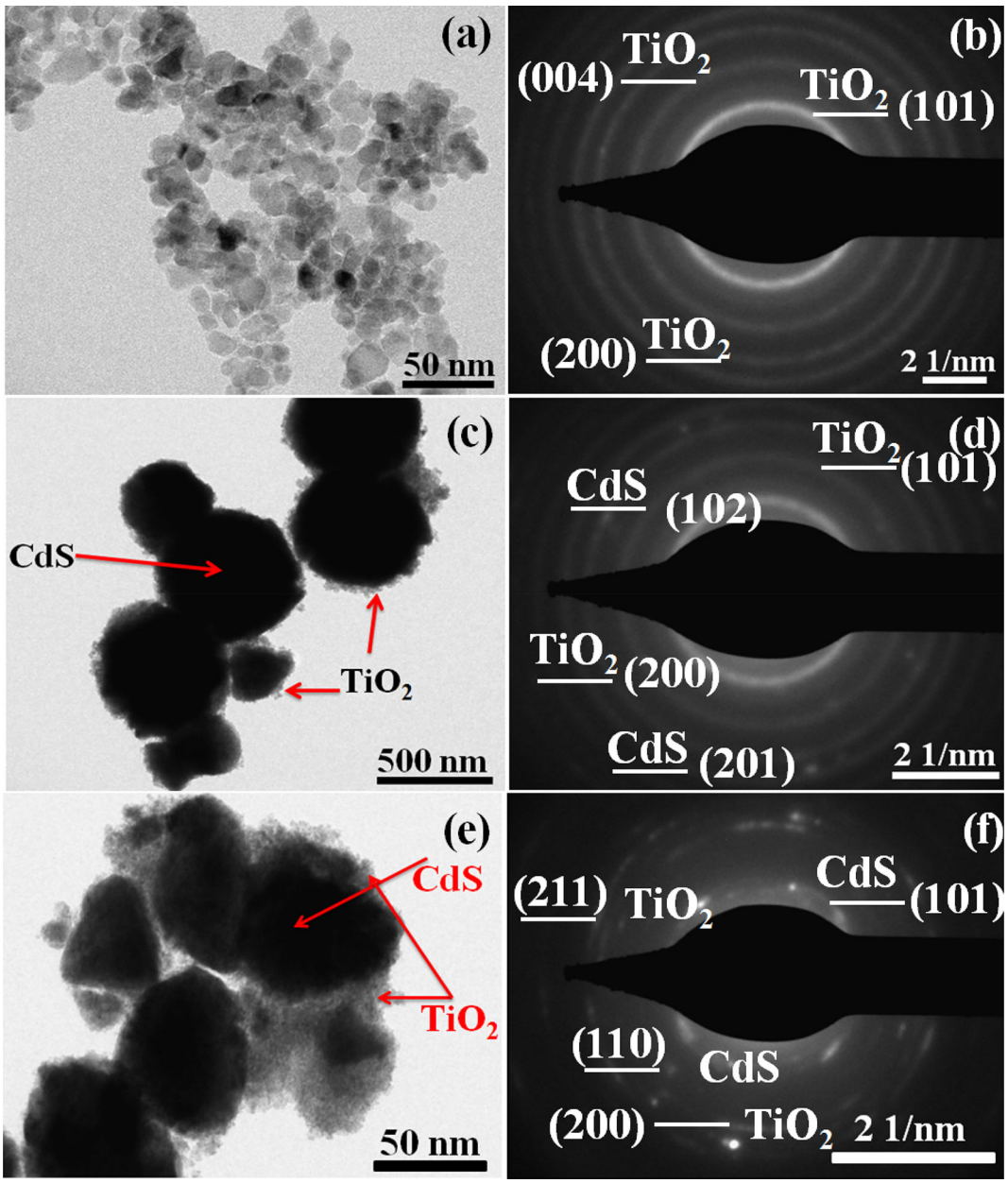


**Figure 3.** (**a**, **c**, **e**) TEM images of as-synthesized bare $TiO_2$ NPs, CT1 and CT2 nanocomposites and (**b**, **d**, **f**) their corresponding SAED patterns.

162.21 and 168.71 eV binding energies corresponding to S $2p_{3/2}$ and S $2p_{1/2}$, respectively [22,38,45].

The UV–Vis diffused reflectance spectra (UV–DRS) of as-prepared bare $TiO_2$ NPs, CT1 and CT2 nanocomposites are shown in figure 6a. It is seen that the $TiO_2$ NPs have absorption edge around at 392 nm with $E_g$ = 3.16 eV, indicating that bare $TiO_2$ NPs have no optical absorption in visible region. CdS has smaller band gap ($E_g$ = 2.42 eV) and absorbs largely in the visible region. The combination of $TiO_2$ and CdS in CT nanocomposites are found to shift absorption band edges predominantly making them suitable for their use as photocatalysts. This results in the increase in their photocatalytic activity. This can be attributed to the synergistic effect of photosensitization of CdS [39]. The CT nanocomposites shows the sharp absorption band edge at ∼528 nm for CT1 and 533 nm for CT2, with a distinct shoulder at 461 nm (figure 6a). The optical absorption spectrum of CT nanocomposites is slightly red-shifted with respect to bulk CdS (512 nm) [46]. Figure 6b shows corresponding band gap of bare $TiO_2$ NPs (3.16 eV),

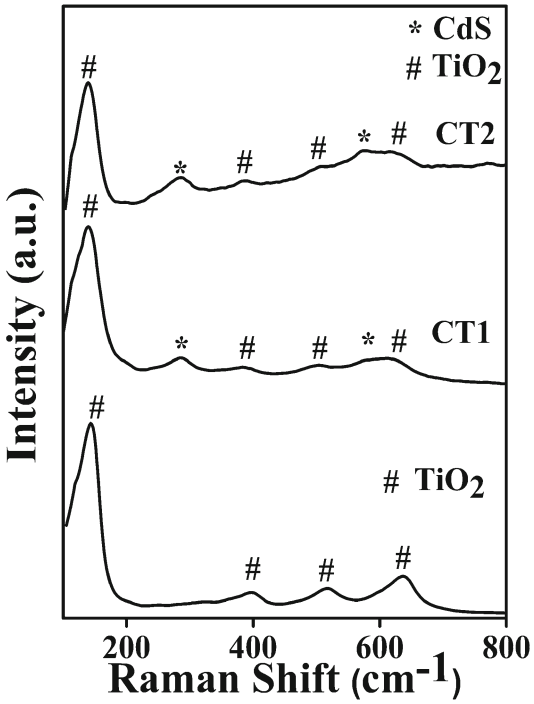


**Figure 4.** Raman spectra of as-synthesized bare $TiO_2$ NPs, CT1 and CT2 nanocomposites.

and nanocomposites (CT1 (2.34 eV) and CT2 (2.32 eV)). The shifts in the band gap are observed from 3.16 to 2.32 eV. The introduction of CdS in nanocomposites (CT1 and CT2) shifts absorption spectra into visible region because CdS has efficient visible light harvesting efficiency. This is because electrons from its valence band get excited and go to the conduction band of $TiO_2$, which further increases the electron–hole pair separation efficiency.

In addition, $N_2$ adsorption–desorption studies were carried out, using Brunauer–Emmett–Teller (BET) equation to calculate the specific surface areas of $TiO_2$ NPs and CT1, CT2 nanocomposites. It was observed that due to formation of CdS@$TiO_2$ nanocomposites (CT), the specific surface area of nanocomposites decreases as compared to bare $TiO_2$ nanoparticles [7,47]. The specific surface area observed for $TiO_2$ NPs and CT1, CT2 nanocomposites were found to be 68.12, 44.04 and 33.88 $m^2\ g^{-1}$, respectively. The obtained results are in agreement with XRD, FESEM and TEM analyses. CdS@$TiO_2$ nanocomposites have larger particle size as compared to $TiO_2$ NPs resulting in decreased surface areas. CdS/$TiO_2$ heterojunction formation gives rise to efficient charge separation [47].

The photodegradation takes place as the photogenerated electrons reacts with adsorbed $O_2^-$ and $OH^-$ radicals. These radicals are highly reactive and they are responsible for degradation of RhB dye. Also, the holes present in the valence band of CdS reacts with $H_2O$ and $OH^-$ producing $OH^\bullet$, which are responsible for degradation of RhB in photocatalytic degradation and produces $CO_2$ and $H_2O$ [1]. The proposed mechanism of photocatalytic degradation of RhB using CdS@$TiO_2$ nanocomposites is shown in figure 7.

This mechanism is further substantiated by PL spectral studies. PL spectra have been recorded to investigate the charge separation efficiency of the materials. Figure 8 shows PL spectra of bare $TiO_2$ NPs and CT nanocomposites. All samples show two strong emission bands at 402 and 428 nm, which are emission bands of $TiO_2$ nanoparticles. The CT nanocomposites shows additional emission band in the red region at 500–600 nm which is attributed to CdS nanocrystals, which is absent in the emission spectrum of $TiO_2$ NPs. This confirms the successful formation of CdS@$TiO_2$ nanocomposites. The PL emission intensity of CT nanocomposites is lower as compared to $TiO_2$ NPs. It indicates the enhanced charge separation, lower electron hole–pair recombination and increased photocatalytic activity of CT nanocomposites [48,49].

The photodegradation of RhB under solar light irradiation ($\lambda$ = 553 nm) was used to study the performance of photocatalysts. It has been observed that the CT nanocomposites shows excellent photocatalytic activity for degradation of RhB as compared to bare $TiO_2$ NPs. After 60 min, CT1 shows 98.74% (figure 9a) and CT2 shows 91.81% (supplementary figure S6b) degradation of RhB, which is much higher than bare $TiO_2$ NPs (66.40%, supplementary figure S6a). In the presence of CT nanocomposites, intensity of the absorption band of RhB at 553 nm decreases with increase in the time of irradiation. It has been observed that the maximum absorption wavelength of RhB has been remarkably blue-shifted due to the decomposition of RhB chromophoric structure [50,51]. Figure 9a shows that the maximum absorption wavelength is shifted to 536 nm after 30 min of irradiation under solar light. Further, with increasing irradiation time (45 min), the absorption band is shifted to 498 nm, it is due to removal of ethyl group [50,52]. As irradiation time increases, intensity of absorption band at 498 nm further decreases and reaches almost zero after 60 min and the dye solution becomes colourless. This reveals that the chromophoric structure of RhB is destroyed.

When CdS is excited, due to narrow band gap energy (2.42 eV), it produces electron–hole pairs. The conduction band (CB) of $TiO_2$ is more positive as compared to CB of CdS. Due to this, when electron–hole pair is generated in CdS, electron from CB of CdS is transferred to CB of $TiO_2$. Whereas, photogenerated holes remain in valence band (VB) of CdS. This reduces the electron–hole pair recombination [49,53]. For comparison, the photodegradation efficiency ($C/C_0$) of RhB using bare $TiO_2$ NPs, CT1 and CT2 nanocomposites was calculated (figure 9b). Further, the photocatalytic activity of as-prepared CT1 (CdS@$TiO_2$)

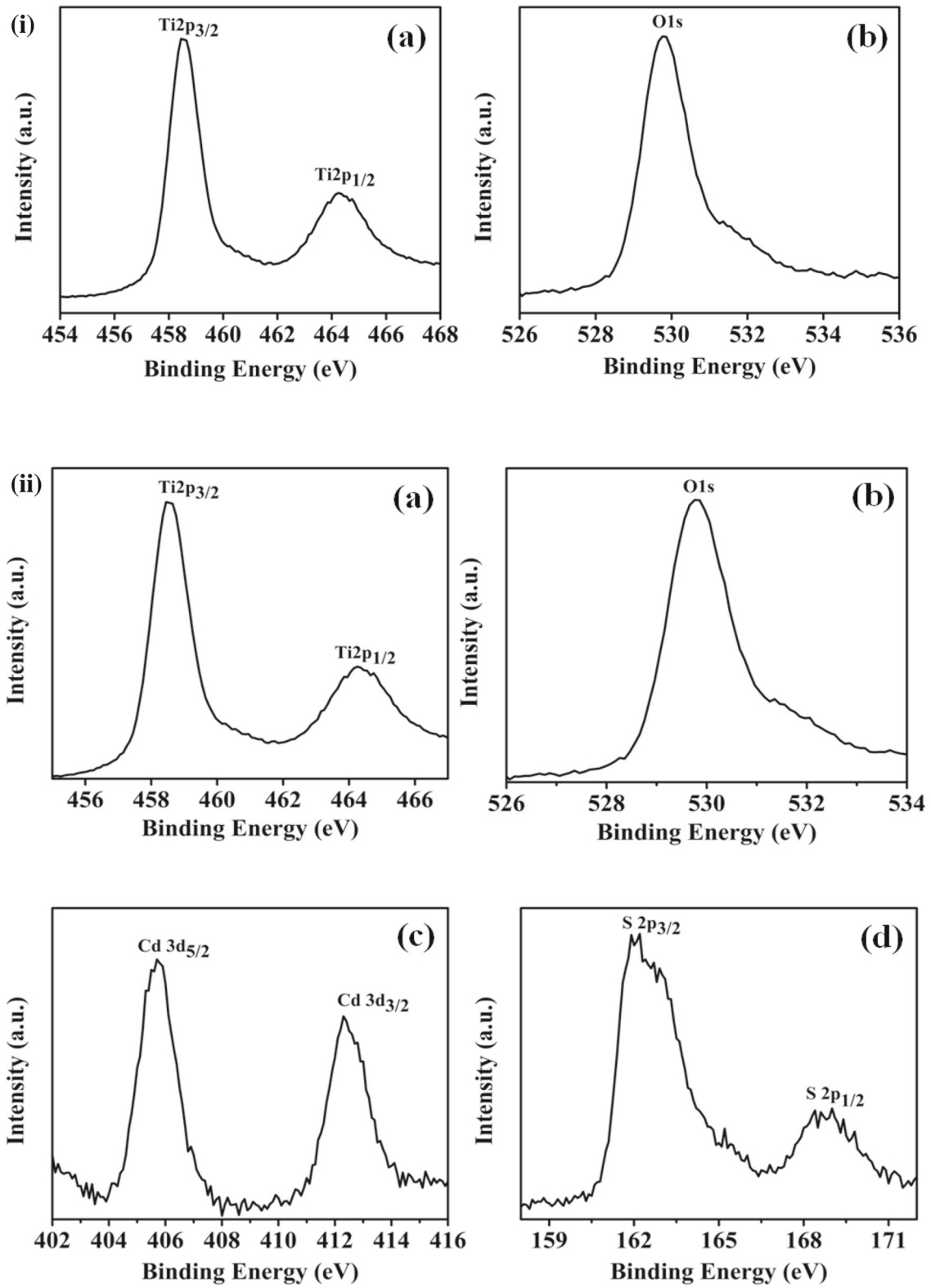


**Figure 5.** (**i**) XPS spectra of as-synthesized bare $TiO_2$ NPs, (**a**) Ti 2p and (**b**) O 1s. (**ii**) XPS spectrum of as-synthesized CT1 nanocomposite, (**a**) Ti 2p, (**b**) O 1s, (**c**) Cd 3d and (**d**) S 2p.

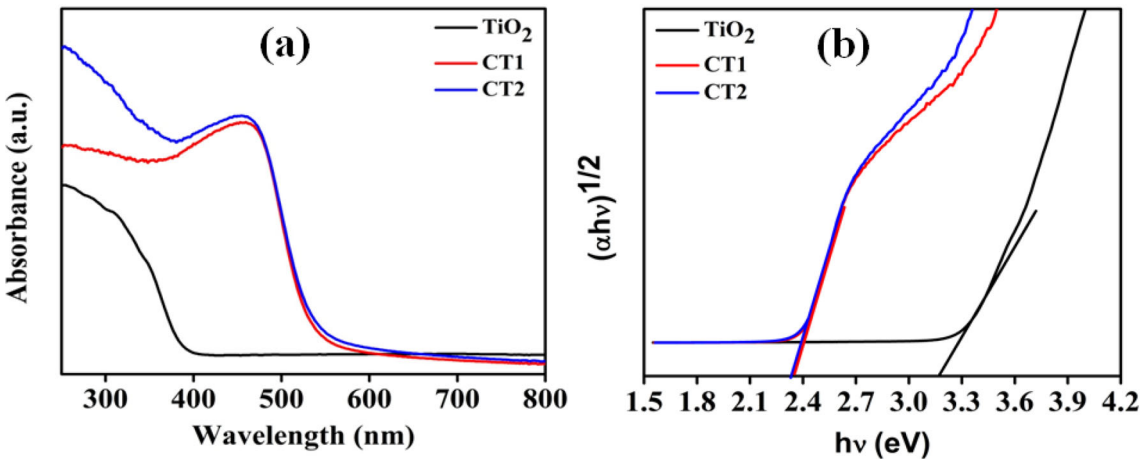


**Figure 6.** (**a**) UV–Vis diffused reflectance spectra and (**b**) Tauc's plot of the as-synthesized bare $TiO_2$ NPs, CT1 and CT2 nanocomposites.

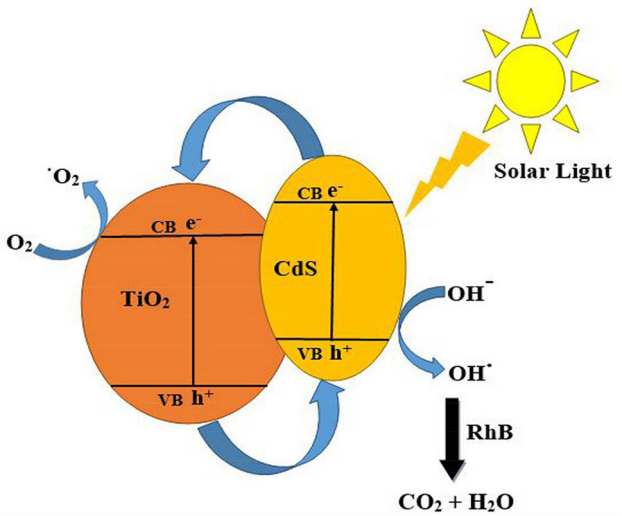


**Figure 7.** The proposed mechanism of photocatalytic degradation of RhB using CdS@$TiO_2$ nanocomposites.

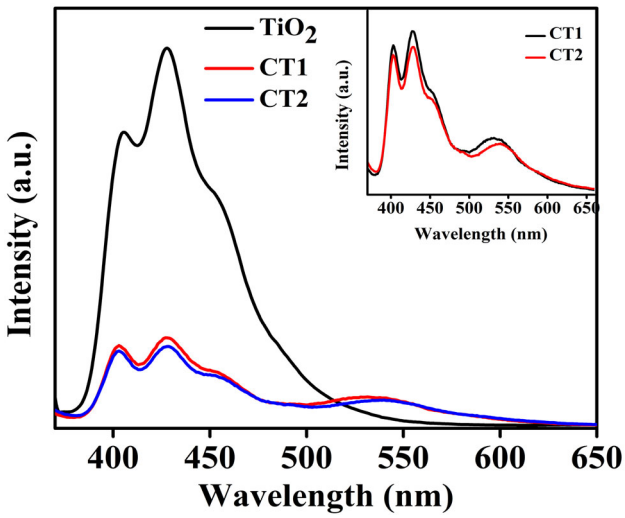


**Figure 8.** Photoluminescence spectra of bare $TiO_2$, CT1 and CT2 nanocomposites.

nanocomposite is compared with activities of the other reported materials (table 1). The recyclability of the as-synthesized CT1 nanocomposite was also performed up to 5 cycles and slight decrease in the efficiency of the nanocomposite has been observed, when compared with the first cycle. The plot of degradation efficiency *vs.* number of cycles is given in figure 9c.

The charge transfer properties of $TiO_2$ and CdS@$TiO_2$ nanocomposites were further studied by CV and EIS in the absence of external source of light. The CV measurements were carried out using 1 M KCl aqueous electrolyte solution at the scan rate of 20 mV $s^{-1}$ in the potential range of 0.0–0.6 V. Figure 10a shows the CV curves of $TiO_2$, CT1 and CT2. The CT nanocomposites exhibit highest peak current observed for the forward and reverse scans. The enhancement of peak current of CT, compared to bare $TiO_2$ nanoparticles, indicates increase in the rate of electron transfer by introduction of CdS. This is well supported by EIS analysis. EIS was studied in the absence of sunlight. Figure 10b shows the Nyquist plots to investigate the charge transfer carriers of bare $TiO_2$, CT1 and CT2 NCs. It was found that CT nanocomposites have smaller semicircles at higher frequency compared to bare $TiO_2$ nanoparticles. It suggests the improved charge transfer in CdS@$TiO_2$ nanocomposites due to the presence of CdS and decreases the electron hole–pair recombination, which is well supported by PL spectrum [54–56].

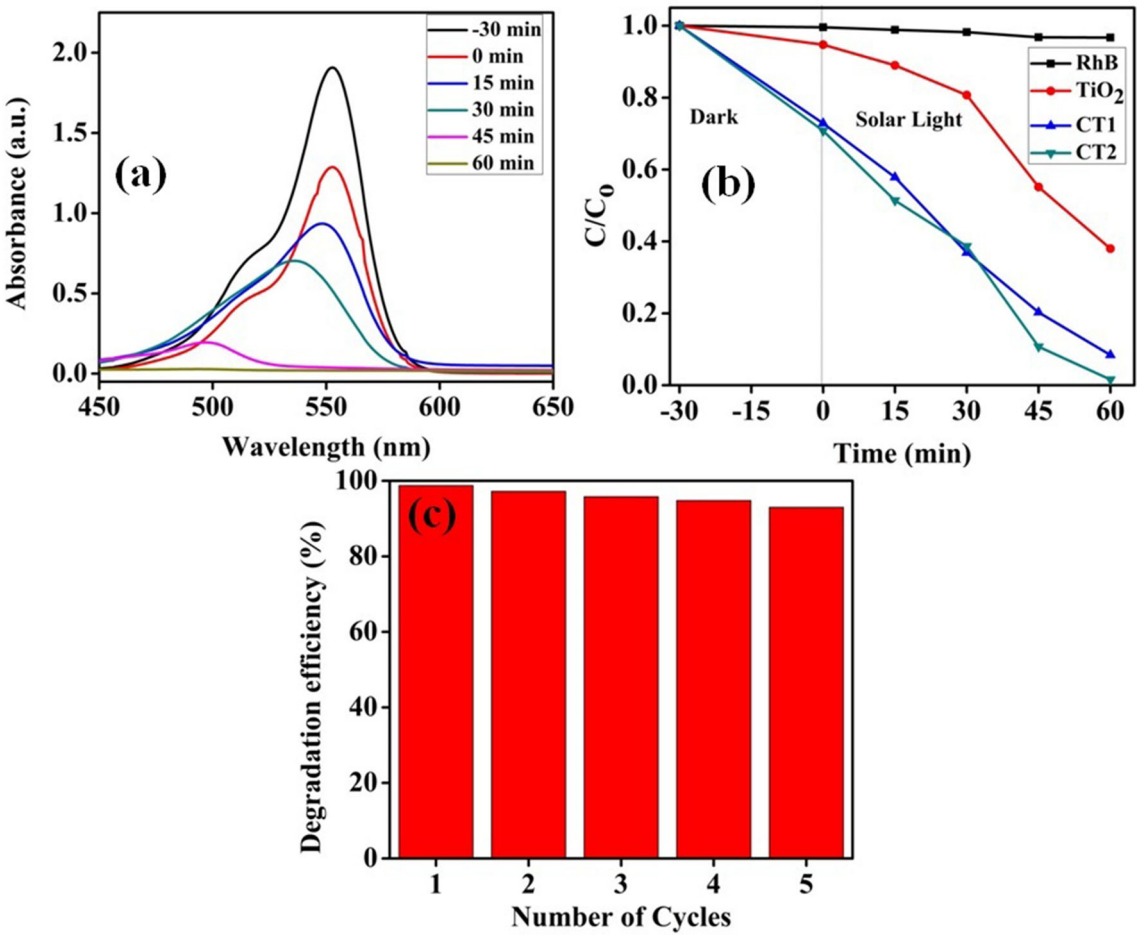


**Figure 9.** (**a**) UV–Vis spectra of RhB during photocatalytic degradation under solar light by as-synthesized CT1 nanocomposite, (**b**) $C/C_0$ *vs.* time for photocatalytic efficiency of RhB under solar light irradiation and (**c**) plot of degradation efficiency *vs*. number of cycles.

**Table 1.** Comparison table of as-prepared CT1 (CdS@$TiO_2$) NCs with reported photocatalysts used for the degradation of RhB.

| Nanocomposites | Dye | Time duration (min) | Irradiation source | References |
|---|---|---|---|---|
| CdS/TNTs | RhB | 120 | 300 W Xe lamp | [21] |
| CdS@$TiO_2$ HDNPs | RhB | 90 | 500 W Xe lamp | [57] |
| CdS/$TiO_2$ | RhB | 140 | 300 W Xe lamp | [40] |
| CdS-a/$TiO_2$ | RhB | 140 | 500 W Xe lamp | [58] |
| CdS/$TiO_2$-20 | RhB | 150 | 300 W Xe lamp | [59] |
| $TiO_2$/CdS | RhB | 100 | 400 W metal halide lamp | [54] |
| $TiO_2$@CdS-6 | RhB | 120 | 300 W Xe lamp | [60] |
| CdS/$TiO_2$ | RhB | 120 | 300 W Xe lamp | [61] |
| CdS/$TiO_2$ | RhB | 420 | 500 W Xe lamp | [62] |
| $TiO_2$-CdS | RhB | 120 | 500 W mercury vapour lamp | [63] |
| $TiO_2$/CdS | RhB | 180 | 500 W Xe lamp | [17] |
| CdS@$TiO_2$ (CT1) | RhB | 60 | Solar light | This work |

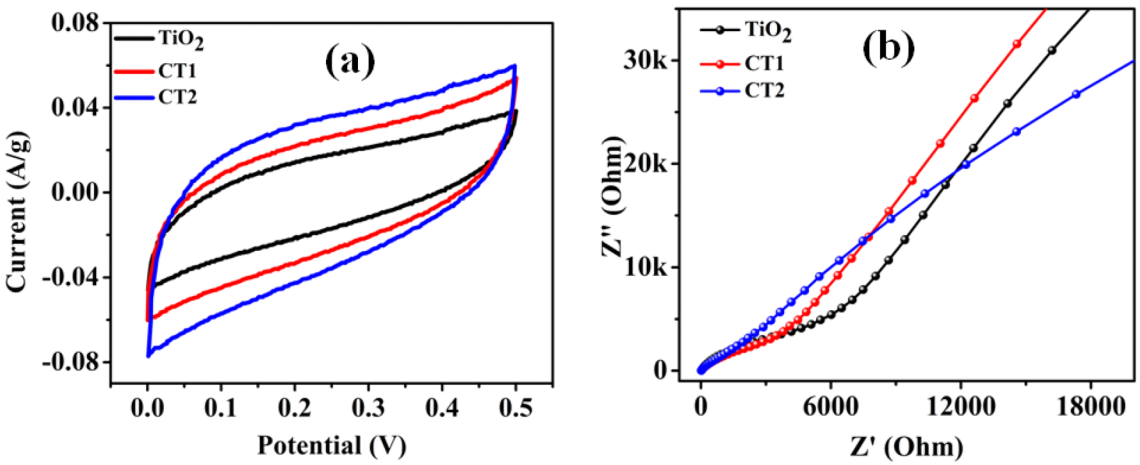


**Figure 10.** (**a**) CV curves and (**b**) Nyquist plots of $TiO_2$, CT1 and CT2 nanocomposites.

## 4. Conclusions

CdS@$TiO_2$ (CT) nanocomposites were successfully synthesized by solvothermal method using bare $TiO_2$ NPs and $CdCl_2$(3-Cl-benzaldehyde thiosemicarbazone)$_2$ as a molecular precursor. The band gap was calculated using Tauc's plot and it was found to shift from 3.16 in $TiO_2$ to 2.32 eV in nanocomposites. It suggests the shift of absorption band edge in composites towards visible region compared to UV region for $TiO_2$ NPs. The as-prepared CT nanocomposites show very efficient photocatalytic activity towards RhB dye degradation under solar light irradiation. The photocatalytic degradation using CT1 and CT2 nanocomposites achieves higher RhB degradation (98.74 and 91.81%, respectively) as compared to bare $TiO_2$ NPs (66.40%) within 60 min. It has been observed that the CT nanocomposites can completely bleach the 10 mg $l^{-1}$ RhB aqueous solution dye under solar light irradiation. The photocatalytic mechanism was studied by PL, CV and EIS. These studies show high charge transfer efficiency for the CT nanocomposites as compared to bare $TiO_2$ NPs and enhanced photocatalytic efficiency. The as-synthesized nanocomposites are promising photocatalytic materials that have good potential for purification of industrial waste water. The main advantage of this type of photocatalysts is that they show photocatalytic activity simply in the presence of sunlight.

## Acknowledgements

We are thankful to the Department of Science and Technology (DST-EMRF grant nos. EMR/2016/007052 and DST-PURSE), India, for providing financial support. We also acknowledge Department of Earth Science, Indian Institute of Technology, Bombay, for providing Raman Facility and MNIT, Jaipur, for providing XPS analysis.

## References

[1] Arabzadeh A and Salimi A 2016 *J. Colloid Interface Sci.* **479** 43
[2] Pant B, Barakat N A M, Pant H R, Park M, Saud P S, Kim J W *et al* 2014 *J. Colloid Interface Sci.* **434** 159
[3] Su C, Shao C and Liu Y 2011 *J. Colloid Interface Sci.* **359** 220
[4] Nakata K and Fujishima A 2012 *J. Photochem. Photobiol. C: Photochem. Rev.* **13** 169
[5] Hoffmann M R, Martin S T, Choi W and Bahnemann D W 1995 *Chem. Rev.* **95** 69
[6] Wang H, Wang G, Ling Y, Lepert M, Wang C, Zhang J Z *et al* 2012 *Nanoscale* **4** 1463
[7] Li X, Chen X, Niu H, Han X, Zhang T, Liu J *et al* 2015 *J. Colloid Interface Sci.* **452** 89
[8] Isamail A A and Bahnemann D W 2011 *J. Mater. Chem.* **21** 11686
[9] Guo X, Di W, Chen C, Liu C, Wang X and Qin W 2014 *Dalton Trans.* **43** 1048
[10] Cao Y, He T, Chen Y and Cao Y 2010 *J. Phys. Chem. C* **114** 3627
[11] Anpo M and Takeuchi M 2003 *J. Catal.* **216** 505
[12] Kato H and Kudo A 2002 *J. Phys. Chem. B* **106** 5029
[13] Iwasaki M, Hara M, Kawada H, Tada H and Ito S 2000 *J. Colloid Interface Sci.* **224** 202
[14] Zhang Z, Shao C, Li X, Sun Y, Zhang M, Mu J *et al* 2013 *Nanoscale* **5** 606
[15] Chaguetmi S, Mammeri F, Nowak S, Decorse P, Lecoq H, Gaceur M *et al* 2013 *RSC Adv.* **3** 2572
[16] Ashokkumar M 1998 *Int. J. Hydrog. Energy* **23** 427
[17] Xue C, Wang T, Yang G, Yang B and Ding S 2014 *J. Mater. Chem. A* **2** 7674
[18] Bessekhouad Y, Robert D and Weber J V 2004 *J. Photochem. Photobiol. A: Chemistry* **163** 569
[19] Shi J-W, Yan X, Cui H-J, Zong X, Fu M-L, Chen S *et al* 2012 *J. Mol. Catal. A: Chem.* **356** 53
[20] Liu Z, Fang P, Wang S, Gao Y, Chen F, Zheng F *et al* 2012 *J. Mol. Catal. A: Chem.* **363** 159
[21] Yu L, Wang D and Ye D 2015 *Sep. Purif. Technol.* **156** 708

[22] Zhou P, Le Z, Xie Y, Fang J and Xu J 2017 *J. Alloys Compd.* **692** 170
[23] Ahmed R, Will G, Bell J and Wang H 2012 *J. Nanoparticle Res.* **14** 1
[24] Lv J, Wang H, Gao H, Xu G, Wang D, Chen Z *et al* 2015 *Surf. Coat. Technol.* **261** 356
[25] Pawar A S, Garje S S and Revaprasadu N 2016 *Mater. Chem. Phys.* **183** 366
[26] Samant K M, Suroshe S J and Garje S S 2014 *Eur. J. Inorg. Chem.* **2014** 499
[27] Ansari A, Badhe R A and Garje S S 2019 *ACS Omega* **4** 14937
[28] Pawar A S, Mlowe S, Garje S S, Akerman M P and Revaprasadu N 2017 *Inorg. Chim. Acta* **463** 7
[29] Disale S D and Garje S S 2011 *J. Organomet. Chem.* **696** 3328
[30] Badhe R A, Ansari A and Garje S S 2018 *ACS Omega* **3** 18663
[31] Ansari A, Sachar S and Garje S S 2018 *New J. Chem.* **42** 13358
[32] Liu L, Luo C, Xiong J, Yang Z, Zhang Y, Cai Y *et al* 2017 *J. Alloys Compd.* **690** 771
[33] Mlondo S N, Revaprasadu N, Christian P, Helliwell M and O'Brien P 2009 *Polyhedron* **28** 2097
[34] Kalpana D, Omkumar K S, Kumar S S and Renganathan N G 2006 *Electrochim. Acta* **52** 1309
[35] Li X, Xia T, Xu C, Murowchick J and Chen X 2014 *Catal. Today* **225** 64
[36] Zhao H, Liu L, Andino J M and Li Y 2013 *J. Mater. Chem. A* **1** 8209
[37] Chen Z and Xu Y J 2013 *ACS Appl. Mater. Interfaces* **5** 13353
[38] Mani A D and Subrahmanyam C 2016 *Mater. Res. Bull.* **73** 377
[39] Wu L, Yu J C and Fu X 2006 *J. Mol. Catal. A: Chem.* **244** 25
[40] Yang G, Yang B, Xiao T and Yan Z 2013 *Appl. Surf. Sci.* **283** 402
[41] Kim Y, Lee J, Jeong H, Lee Y, Um M H, Jeong K M *et al* 2008 *J. Ind. Eng. Chem.* **14** 396
[42] Li X, Shen H, Li S, Niu J Z, Wang H and Li L S 2010 *J. Mater. Chem.* **20** 923
[43] Sun M, Wang Y, Fang Y, Sun S and Yu Z 2016 *J. Alloys Compd.* **684** 335
[44] Qorbani M, Naseri N, Moradlou O, Azimirad R and Moshfegh A Z 2015 *Appl. Catal. B: Environ.* **162** 210
[45] Kozlova E A, Kozhevnikova N S, Cherepanova S V, Lyubina T P, Gerasimov E Y, Kaichev V V *et al* 2012 *J. Photochem. Photobiol. A: Chem.* **250** 103
[46] Bruce J C, Revaprasadu N and Koc K R 2007 *New J. Chem.* **31** 1647
[47] Maleki M and Haghighi M 2016 *J. Mol. Catal. A: Chem.* **424** 283
[48] Onwudiwe D C, Kruger T P J, Oluwatobi O S and Steydom C A 2014 *Appl. Surf. Sci.* **290** 18
[49] Jostar T S, Devadason S and Suthagar J 2015 *Mater. Sci. Semicond. Process.* **34** 65
[50] Fu H, Pan C, Yao W and Zhu Y 2005 *J. Phys. Chem. B* **109** 22432
[51] Guo X, Chen C, Song W, Wang X, Di W and Qin W 2014 *J. Mol. Catal. A: Chem.* **387** 1
[52] Zhou L, Jin C, Yu Y, Chi F, Ran S and Lv Y 2016 *J. Alloys Compd.* **680** 301
[53] Zhao H, Wu M, Liu J, Deng Z, Li Y and Su B-L 2016 *Appl. Catal. B: Environ.* **184** 182
[54] Wang M, Zhang H, Zu H, Zhang Z and Han J 2018 *Appl. Surf. Sci.* **455** 729
[55] Li C, Fan W, Lu H, Ge Y, Bai H and Shi W 2016 *New J. Chem.* **40** 2287
[56] Divya K S, Xavier M M, Vandana P V, Reethu V N and Mathew S 2017 *New J. Chem.* **41** 6445
[57] Sun G, Zhu C, Zheng J, Jiang B, Yin H, Wang H *et al* 2016 *Mater. Lett.* **166** 113
[58] Liang H, Liu S, Zhang H, Wang X and Wang J 2018 *RSC Adv.* **8** 13625
[59] Tian F, Hou D, Hu F, Xie K, Qiao X and Li D 2017 *Appl. Surf. Sci.* **391** 295
[60] Shi Z, Liu J, Lan H, Li X, Zhu B and Yang J 2019 *J. Mater. Sci.: Mater. Electron.* **30** 17682
[61] Dang R and Ma X 2017 *J. Mater. Sci.: Mater. Electron.* **28** 8818
[62] Wang H, Li J, Zhou H, Yao S and Zhang W 2019 *J. Mater. Sci.: Mater. Electron.* **30** 10754
[63] Yang H, Liu Z, Wang K, Pu S, Yang S and Yang L 2017 *Catal. Lett.* **147** 2581